Journal of proteome research

pubs.acs.org/jpr

Article

Applying Untargeted Lipidomics to Evaluate the Efficacy of Combined Neoadjuvant Chemotherapy and Immunotherapy for Esophageal Squamous Carcinoma Treatment

Weijie Lin,[§] Xianzhe Si,[§] Zhihuang Zhao, Feng Chen, Jie Xu, Wenbo Huang, Jianqing Lin, Zhiyao Chen,* and Zhijun Huang*

Cite This: https://doi.org/10.1021/acs.jproteome.3c00527

Read Online

ACCESS | Metrics & More | Article Recommendations

ABSTRACT: Esophageal squamous cell carcinoma (ESCC) is an aggressive malignant tumor with a poor prognosis due to insidious symptoms that make early diagnosis difficult. Despite the combination of multiple treatment modalities, the recurrence and mortality rates of ESCC remain high. Neoadjuvant chemotherapy combined with immunotherapy is an emerging treatment modality that improves the prognosis of patients with ESCC. However, owing to the presence of hyperprogression and pseudoprogression, the currently used methods cannot accurately evaluate the efficacy of this therapy in patients, thus creating an evaluation bias and depriving these patients of the opportunity to benefit. We used untargeted lipidomics to identify the differences in lipid composition between cancer specimens and normal tissue specimens in the neoadjuvant chemotherapy combined with the immunotherapy group and the surgery-alone group of esophageal cancer patients and constructed a prediction model based on sphingomyelin 12:1;2O/30:0 and triglyceride (TG) 60:3 | TG 18:0_24:1_18 using a machine learning approach, which helps to better evaluate the neoadjuvant efficacy of combination therapy and better guide the treatment of ESCC.

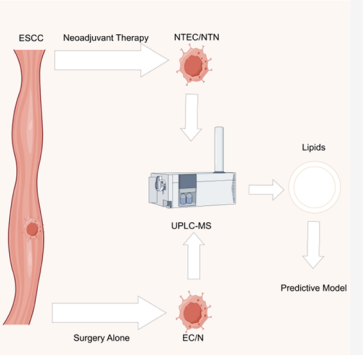

KEYWORDS: *esophageal squamous cell carcinoma, lipid metabolism, untargeted lipidomics, efficacy evaluation*

INTRODUCTION

Esophageal cancer is among the top ten cancers in terms of incidence and mortality worldwide, and China reports the highest incidence of esophageal cancer. Regarding histological typing, nearly 90% of esophageal cancers are esophageal squamous cell carcinomas (ESCCs), while the remaining cases are esophageal adenocarcinomas (EACs).[1] The early symptoms of esophageal cancer mainly include progressive dysphagia; therefore, disease onset is relatively insidious, and patients are unaware they have it. Consequently, esophageal cancer is usually diagnosed during the intermediate and advanced stages, and the recurrence rate in patients is greater than 40%. The five-year survival rate is less than 20%;[2] therefore, improving the treatment efficacy and prognosis of patients with esophageal cancer has been widely studied. The primary treatment for esophageal cancer is comprehensive treatment based on surgery, and chemotherapy, tumor radiation therapy, targeted therapy, and immunotherapy are often used as adjuvant treatments for esophageal cancer.[3] In recent years, the multidisciplinary treatment concept has been widely recognized in the treatment of esophageal cancer because patients with intermediate- and advanced-stage esophageal cancer cannot be cured with surgery alone. Neoadjuvant chemotherapy combined with immunotherapy has been shown to improve the R0 resection and step-down rates compared with neoadjuvant chemotherapy alone, making it an essential treatment for patients with intermediate and advanced-stage esophageal cancer.[4]

In recent years, immunotherapy has significantly improved the survival rates of patients with cancer.[5] Phase II and III trials have shown improved survival rates in patients with esophageal cancer treated with immune checkpoint inhibitors.[6−78] Neoadjuvant immunotherapy can effectively improve the pCR rate in patients compared with that in patients treated with neoadjuvant chemotherapy, indicating that the combination of neoadjuvant chemotherapy and immunotherapy is beneficial for patients with esophageal cancer. For example, the overall survival of patients with ESCC treated with pembrolizumab and chemotherapy is better than that of patients treated with chemotherapy alone.[9]

Received: August 22, 2023
Revised: December 4, 2023
Accepted: December 22, 2023

Lipids are not only the main building blocks of cell membranes but also the main source of energy in the body. In addition, they are involved in the formation of signal transduction networks and in the regulation of intercellular signaling. Enhanced lipid synthesis or uptake contributes to rapid cancer cell growth and distant tumor metastasis.[13] Accumulated data suggest that tumor and immune cells have abnormalities in cellular energy metabolism during tumorigenesis and progression.[10] For example, impaired lipid metabolism in immune cells is essential for coordinating immunosuppression and tumor immune escape.[11] Chen et al. demonstrated that excess lipids in obese patients impair natural killer cell-mediated immune surveillance, thereby promoting the immune escape of cancer cells.[12] Batista-Gonzalez et al. have shown that lipid metabolism plays a key role in the activation of M1 and M2 macrophages.[13] Lipid abnormalities in immune cells disrupt the tumor microenvironment balance and may promote the immune escape of the tumor cells.

In recent years, tumor lipid metabolomics has been a new field receiving considerable attention. Currently, lipidomics analysis is generally performed using liquid chromatography−mass spectrometry (LC−MS), which is classified into two categories: untargeted and targeted analyses.[13] Lipid metabolomics is widely used to identify biomarkers for various cancers. For example, Luo et al. successfully identified plasma biomarkers using lipidomics to accurately diagnose pancreatic cancer during the early stages of the disease.[14] Ecker et al. found that triglycerides may be potential biomarkers of colorectal cancer.[15] Yang et al. used lipidomics to confirm that glycerophospholipid metabolism promotes ESCC progression.[16] Lin et al. used LC−MS to identify potential markers for renal cell carcinoma.[17] Untargeted ultra-high-performance liquid chromatography (UPLC-MS) analysis has better analytical speed, separation, and detection sensitivity than LC−MS analysis and is widely used in pharmaceutical analysis for cardiovascular disease treatment.[18] Therefore, lipidomics is a feasible and reliable experimental method, and untargeted lipidomics can help screen for statistically significant differential lipid molecules.

This study analyzed lipid differences between esophageal cancer patients in the group receiving neoadjuvant and those in the surgery-only group using the UPLC-MS QE Plus platform and constructed a predictive model based on differential lipids, which will hopefully contribute to a better prediction of the efficacy of immunotherapy in patients with ESCC, thereby improving their 5-year survival and decreasing the recurrence rate.

METHODS

Apparatus and Reagents

The instruments and reagents used are summarized in Table 1.

Table 1. Experimental Apparatus and Models Used in This Study

instrument	manufacturer	model
mass spectrograph	Thermo Scientific	Q Exactive Plus
ultra-high-pressure liquid chromatograph	Shimadzu	Nexera X2 LC-30AD
chromatographic column	Waters	Waters Acquity UPLC HSS C18 column (1.9 μm 2.1 × 100 mm)
ultrasonic wave system	Diagenode	Bioruptor
vacuum centrifuge concentrator	Eppendorf	Concentrator plus
centrifugal machine	Eppendorf Centrifuge	5430R
centrifugal machine	Eppendorf	Centrifuge 5424R
visible ultraviolet spectrophotometer	Thermo	MultiSkan FC
acetonitrile	Millipore	1.00030.4008
methyl alcohol	Millipore	1.06007.4008
ammonium hydroxide	Merck	105,426
ammonium acetate	Sigma	73,594
formic acid	Millipore	111,670
MTBE	Merck	34,875

Study Design and Participants

Thirty-nine samples were collected from patients with ESCC treated with a combination of neoadjuvant chemotherapy and immunotherapy. After screening, 10 patients in the neoadjuvant therapy group were included in our trial. In addition, we randomly selected 10 patients who underwent surgery alone. Twenty patients with ESCC from the Second Hospital of Fujian Medical University were included in our trial, and those who underwent multiple (greater than three) neoadjuvant treatments, underwent chemotherapy, had previous surgery, or had hypertension, diabetes mellitus, or metabolic syndrome were excluded. Surgical specimens, including cancerous and normal tissues, were collected from 20 patients for a total of 40 samples and divided into four groups in the following order: cancerous tissue in the neoadjuvant treatment group of ESCC (NTEC), normal tissue in the neoadjuvant treatment group of ESCC (NTN), cancerous tissue in the surgery-alone group of ESCC (EC), and normal tissue in the surgery-alone group of ESCC (N). Among these, NTEC and NTN groups are collectively referred to as neoadjuvant chemotherapy combined with the immunotherapy group (hereafter referred to as the neoadjuvant treatment group). The EC and N groups are collectively referred to as the surgery-only group. For patients with ESCC, the diagnosis was confirmed by postsurgical pathological examination and tumor staging according to the American Joint Committee on Cancer (AJCC) 8-stage staging system.[19] Basic information such as tumor regression grade, body mass index (BMI), presurgical treatment plan, history of smoking and alcohol, and past medical history were also collected. This study was approved by the Ethics Committee of the Second Affiliated Hospital of Fujian Medical University (protocol code 130; approval date: 2022). The informed consent was signed.

Tissue Collection and Pretreatment

Immediately after isolating the surgical specimen, the samples were thoroughly washed with a 0.9% sodium chloride solution. They were then stored at −80 °C in a refrigerator. For pretreatment, the samples were thawed at 4 °C, and a portion of 57 mg was weighed out. Next, 100 μL of prechilled 75% methanol and three steel beads were added to a shaker for shaking and crushing. Subsequently, 1 mL of prechilled methyl *tert*-butyl ether was added, and the mixture was vortexed and shaken. The mixture was placed at 4 °C in a refrigerator and rotated for 1 h. The samples were then subjected to ultrasonication for 15 min in an ice bath, which was repeated twice. After 100 μL of water was added, the mixture was vortexed and shaken for 1 min and left to stand at 25 °C for 10 min. Centrifugation at 14,000*g* and 4 °C for 15 min allowed for the collection of the upper layer, which contained the lipid fraction. Each sample was then combined with an equal

https://doi.org/10.1021/acs.jproteome.3c00527
J. Proteome Res. XXXX, XXX, XXX−XXX

volume of the lipid fraction, dried using a nitrogen-blowing apparatus, and redissolved in 100 μL of isopropanol/methanol (1/1, v/v). The redissolved samples were transferred to injection vials and stored at low temperatures. Quality control (QC) samples were used to assess the instrument status, evaluate the UPLC-MS system before injection, and ensure system stability throughout the experiment.

UPLC-MS Analysis

The samples were analyzed using a SHIMADZU-LC30 UPLC system with a Waters Acquity UPLC HSS C18 column (1.9 μm 2.1 × 100 mm) obtained from Waters, Milford, MA. The injection volume was 5 μL, and the analysis was conducted at 40 °C with a flow rate of 0.3 mL/min. The mobile phase consisted of two components: (A) a solution of 0.77 g of ammonium formate in acetonitrile and water (nitrile/water = 6:4, v/v) and (B) a solution of acetonitrile and isopropanol (acetonitrile/isopropanol = 1:9, v/v). The gradient elution program was as follows:

0 to 2 min: B changed linearly from 30 to 32%;
Two to 6 min: B changed linearly from 32 to 45%;
Six to 8 min: B changed linearly from 45 to 52%;
Eight to 12 min: B changed linearly from 52 to 58%;
Twelve to 15 min: B changed linearly from 58 to 66%;
Fifteen to 18 min: B remained at 66%;
Eighteen to 21 min: B changed linearly from 66 to 70%;
Twenty-one to 25 min: B remained at 97%;
Twenty-five to 26 min: B changed linearly from 97 to 32%; and
Twenty-six to 30 min: B remained at 32%.

The samples were stored in a 6 °C autosampler throughout the analysis. To minimize the impact of instrument detection signal fluctuations, continuous analysis of the samples was performed randomly. Additionally, a QC sample was included in every 5−7 experimental samples in the queue to monitor and assess the system stability and reliability of the experimental data.

Mass Spectrometry Conditions

Electrospray ionization was employed for detection in both positive and negative ion modes. The UPLC-separated samples were analyzed by using a Q Exactive Plus mass spectrometer (Thermo Scientific). In positive mode, the heater temperature was set to 300 °C, the sheath gas flow rate was 45 arb, the auxiliary gas flow rate was 15 arb, the sweep gas flow rate was 1 arb, the spray voltage was 3.0 kV, the capillary temperature was 350 °C, and the S-Lens RF level was 50%. The scan range for positive mode analysis was 200−1500. In negative mode, the heater temperature was again 300 °C, the sheath gas flow rate was 45 arb, the auxiliary gas flow rate was 15 arb, the sweep gas flow rate was 1 arb, the spray voltage was 3.5 kV, the capillary temperature was 350 °C, and the S-Lens RF level was 50%. The scan range for the negative mode analysis was also 200−1500.

Data Processing

TMSDAIL software (version 4.0.9) was used for lipid identification and quantification. The main parameters were as follows: precursor mass tolerance, 10 ppm; product mass tolerance, 10 ppm; and retention time of 0.1 min for ion peak alignment. Lipid molecules with an RSD of >30% were removed from the QC samples. The data extracted using MSDAIL software were identified, aligned, and normalized to the total peak area. The data were preprocessed using UV scaling for multidimensional and unidimensional statistical analysis.

RESULTS

Clinical Characteristics of Patients

Twenty samples from the neoadjuvant treatment group and 20 from the surgery-alone group were included according to our criteria. Table 2 summarizes the detailed characteristics of the patients, including age, sex, and cancer stage. There were no statistically significant differences between the neoadjuvant therapy and surgery-alone groups in terms of age (p = 0.971), sex (p = 0.141), BMI (p = 0.257), or history of smoking or alcohol consumption (p = 0.141).

Table 2. Clinical Characteristics of Subjects in the Neoadjuvant Therapy Group and Surgery-Alone Group[a]

	neoadjuvant therapy group		surgical alone group		
	NTEC	NTN	EC	N	p
number	10	10	10	10	
Anthropometric Characteristics					
age (years)	62.40 ± 6.96		63.90 ± 0.23		0.971
gender (M/F)	9/1		5/5		0.141
BMI (kg/m^2)	20.10 ± 3.22		20.36 ± 1.62		0.257
history of tobacco and alcohol (Y/N)	9/1		5/5		0.141
TRG					
0	1				
1	5				
2	4				
3	0				
TNM Stages					
I	5		2		
II	1		0		
III	3		7		
IV	0		1		

[a]Abbreviations: BMI, body mass index; TRG, tumor regression grade; NTEC, cancerous tissue in the neoadjuvant treatment group of esophageal squamous carcinoma; NTN, normal tissue in the neoadjuvant treatment group of esophageal squamous carcinoma; EC, cancerous tissue in the surgery-alone group of esophageal squamous carcinoma; N, normal tissue in the surgery-alone group of esophageal squamous carcinoma.

Screening and Defining Differential Metabolites

In total, 1289 lipid compounds were identified by LC−MS/MS analysis using positive and negative ion modes. The spectra of the QC samples were compared for overlap, indicating consistent response intensities and retention times and demonstrating good experimental reproducibility. The peaks from all experimental and QC samples were analyzed using principal component analysis after UV scaling, resulting in closely clustered QC samples, further confirming the reproducibility of the project. Overall, the instrumental analysis system remained stable throughout the experiment, ensuring that reliable data. The observed differences in the lipid profiles reflect biological variations between the samples. Additionally, QC samples were prepared by mixing equal amounts of all samples and calculating the coefficient of variation for each metabolite to assess the data stability and reproducibility.

https://doi.org/10.1021/acs.jproteome.3c00527
J. Proteome Res. XXXX, XXX, XXX−XXX

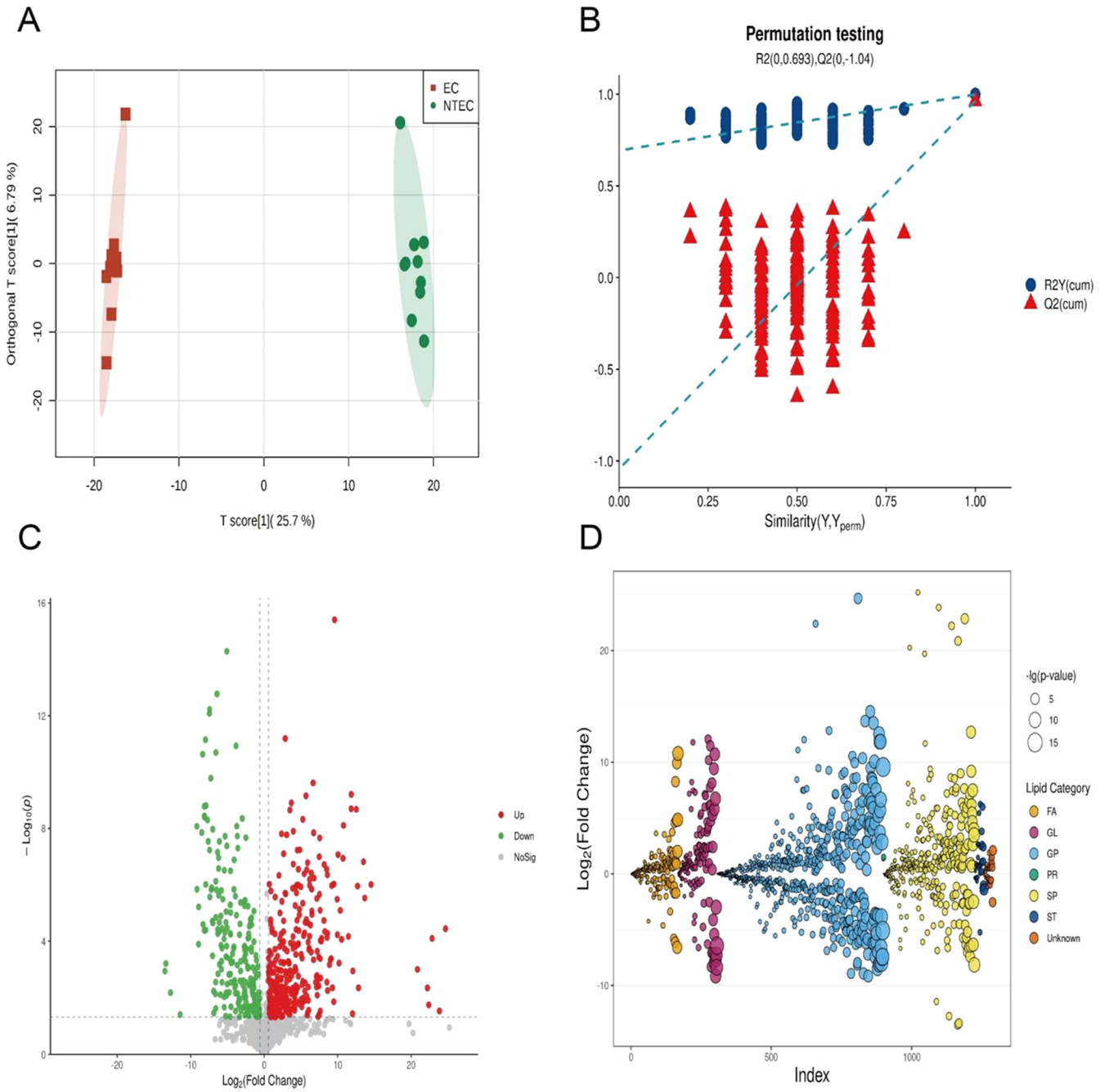

Figure 1. Statistical analysis of the NTEC group vs EC group. (A) OPLS-DA score plot of the NTEC group vs EC group. The red dots represent EC and the green dots represent NTEC. (B) Permutation test chart for OPLS-DA.Q2 Intercept <0.05 represents no overfitting of the model. (C) Volcano plot of VIP values. Red dots indicate lipids with upregulated expression and green dots indicate lipids with upregulated expression. (D) FC and −lg(*p*-value) classification bubble chart. Larger circles indicate larger *p*-values for negative logarithmic transformations, that is, higher significance of differences. Different colors indicate first-class classification, i.e., lipids of the same classification are arranged together.

First, we compared the NTEC and EC groups. Orthogonal partial least-squares discriminant analysis (OPLS-DA) score plots were used to estimate the overall distribution of samples from the neoadjuvant and surgery-alone groups (Figure 1A). A clear separation was observed between the two groups in the OPLS-DA score plots. The OPLS-DA model evaluation parameters obtained were R2 X = 0.325, R2 Y = 0.998, and Q2 = 0.963, indicating the high predictive power of the model. The model was tested using the permutation test (Figure 1B), with Q2 Intercept = −1.043 and Q2 Intercept <0.05, and the model was not overfitted, indicating that it was stable and reliable. Three conditions were used to determine differential metabolites: variable importance in the projection (VIP)>1.0, p < 0.05, FC > 1.5, or FC < 0.667. Accordingly, 488 differential metabolites were identified for subsequent pathway analysis based on the preliminary screening results of the volcano map (Figure 1C). A lipid molecule bubble map (Figure 1D) was also plotted to better represent the degree of variation in the different classifications. Heat maps (Figure 2A) and lipid categorization loops (Figure 2C) were plotted based on these lipids, which were selected as the top 50 lipids based on the magnitude of their VIP values. Heat maps (Figure 2B)

https://doi.org/10.1021/acs.jproteome.3c00527
J. Proteome Res. XXXX, XXX, XXX−XXX

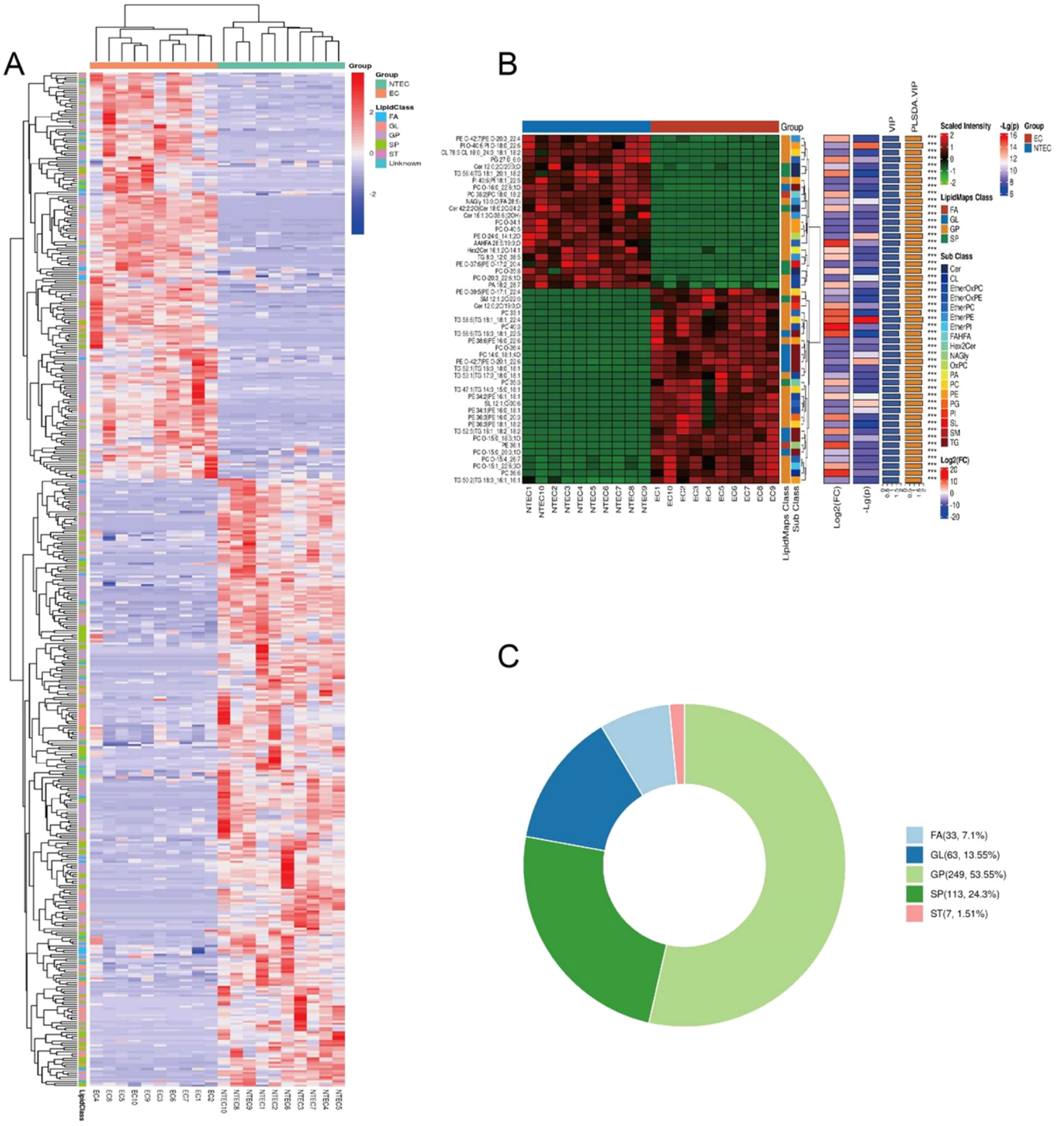

Figure 2. Heat map and lipid classification ring diagram of differential metabolites. (A) Heat map of 488 differential lipids in the NTEC group vs. EC group. (B) Heat map of the top 50 differential lipids according to the VIP value. Red represents the expression of upregulation and green represents the expression of downregulation. (C) Statistical ring diagram of the classification of 488 differential lipids in the NTEC group vs. EC group. The percentage represents the proportion of total lipid species that this lipid species represents.

were plotted to better reflect the expression of the top 50 lipids in different groups. We focused on the top 10 differentially expressed lipids because of the larger number of differentially expressed lipids. The top 10 differentially expressed lipids were phosphatidylcholine (PC) 36:2|PC 18:0_18:2, phosphatidylethanolamine (PE) 36:1, triglyceride (TG) 52:1|TG 16:0_18:0_18:1, PC O-36:4, PC 14:0_18:1;4O, PC O-16:0_22:6;1O, PC O-15:0_20:3;1O, PC O-15:0_ 18:3;1O, PE O-42:7|PE O-20:1_22:6, and TG 52:5|TG 16:1_18:2_18:2. In total, two metabolites were upregulated, and eight metabolites were downregulated among the top 10 lipids; six of these 10 metabolites were PCs, two were PEs, and two were TGs. The major classes of lipids included 80% glycerophospholipids and 20% glycerol lipids. Meanwhile, 75% of the glycerophospholipids were downregulated in the neoadjuvant therapy group. Based on the screened differential metabolites, KEGG metabolic network enrichment analysis was performed to identify disordered metabolic pathways, and f3

https://doi.org/10.1021/acs.jproteome.3c00527
J. Proteome Res. XXXX, XXX, XXX−XXX

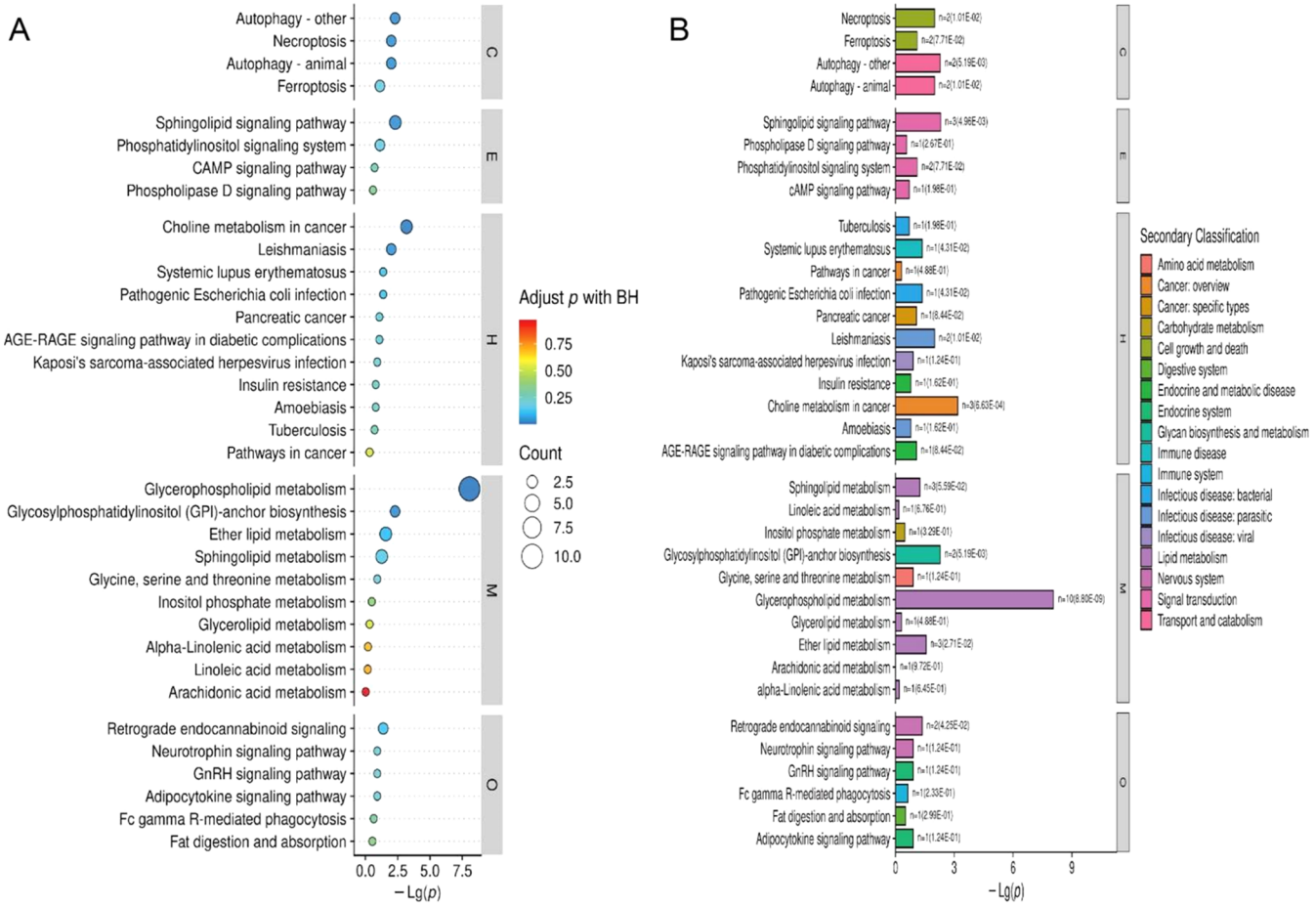

Figure 3. Pathway enrichment analysis of differential lipids. (A) Significant differences in KEGG pathway bubble plots of lipids in the NTEC group vs the EC group. The color of the bubbles indicates significance, and the size of the bubbles represents the number of differential lipids in the pathway where the key lipids are located. (B) Statistical analysis of KEGG enrichment of lipids in NTEC and EC groups. Different colors represent the secondary classification of different metabolic pathways.

the results are presented as bubble plots (Figure 3A). According to the results of this study (Figure 3B), some metabolic pathways were altered differently in the neoadjuvant therapy group compared to the surgery-only group, with the most prominent altered pathways being glycerophospholipid metabolism, choline metabolism in cancer, sphingolipid signaling pathway, glycosylphosphatidylinositol (GPI)-anchored biosynthesis, autophagy—other, autophagy—animal, necroptosis, ether lipid metabolism, retrograde endocannabinoid signaling, and retrograde endogenous cannabinoid signaling. Similarly, we analyzed the NTN and N groups and found that five metabolites were upregulated and five were downregulated among the top 10 differential metabolites. Among these, glycerophospholipids accounted for 60 and 66.7% were downregulated, which were comparable to those in the NTEC and EC groups. KEGG enrichment analysis indicated that several metabolic pathways were altered, including glycerophospholipid metabolism, GPI-anchored biosynthesis, autophagy—other, sphingolipid signaling pathway, ferroptosis, necroptosis, autophagy—animal, choline metabolism in cancer, and lipid metabolism. Finally, we performed multiple comparative analyses between the four groups of the top ten metabolites to determine the variability and found that four metabolites were upregulated and six metabolites were downregulated in the neoadjuvant therapy group compared with the surgery-only group, of which 70% were glycerophospholipids, 20% were glycerolipids, and 10% were sphingolipids. Sphingomyelin (SM) 42:2;2O showed the most significant difference. KEGG enrichment analysis indicated that the altered metabolic pathways included glycerophospholipid metabolism, choline metabolism in cancer, GPI-anchored biosynthesis, autophagy—other, sphingolipid signaling pathway, necroptosis, ether lipid metabolism, and retrograde endocannabinoid signaling the NTEC group vs EC group.

Predictive Model for Efficacy Evaluation

To construct predictive models that can accurately assess the efficacy of neoadjuvant chemotherapy and immunotherapy, we used machine learning methods. Histological data typically contain a large number of variables and samples, and traditional data analysis methods have difficulties handling high-dimensional data. In contrast, machine learning methods can handle high-dimensional data. Complex nonlinear relationships exist in biological systems, and machine learning methods can discover these nonlinear relationships and help screen for biomarkers.

We selected NTEC and EC groups as the data sources for model construction. First, we used differential metabolite data; 488 differential metabolites were detected in the NTEC and EC groups. To identify a specific biomarker, we selected 184 differential metabolites with VIP > 1.5, that is, the features

https://doi.org/10.1021/acs.jproteome.3c00527
J. Proteome Res. XXXX, XXX, XXX−XXX

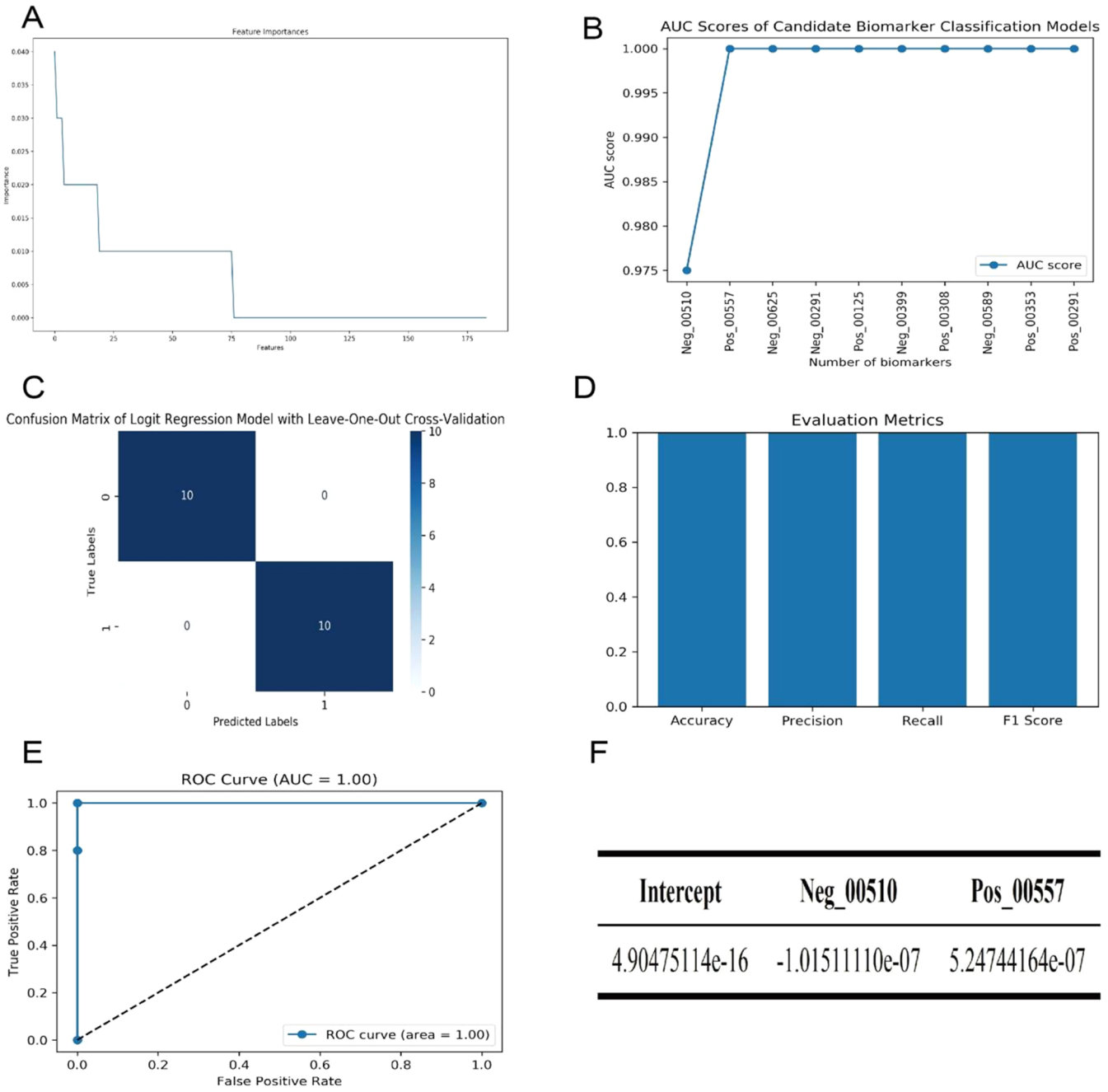

Figure 4. Predictive model building and validation. (A) Random forest model feature importance plot. (B) Candidate marker AUC score cumulative plot. The horizontal coordinate represents the ID of the metabolite. (C) Confusion matrix plot using the leave-one-out logistic regression model. (D) Model evaluation indicator plot. Accuracy: 1.0, precision: 1.0, recall: 1.0, F1 score: 1.0. (E) Model ROC curve plot. AUC: area under the curve. (F) Extracting the trained model parameters based on the receiver operating characteristic map of this predictive model. Neg_00510: SM 12:1;2O/30:0; Pos_00557: TG 60:3|TG 18:0_24:1_18.

from the initial screening. The data set obtained from the primary screening was then divided into training and test sets, labeled as sample categories. Using an integrated learning model, a random forest was used for secondary screening; by visualizing the feature importance of different metabolites in the random forest classification model, as shown in Figure 4A, we screened the top 10 metabolites as our alternative biomarkers, which can navigate to the original data to determine the corresponding metabolites according to the ID of the differential metabolites. We then filtered the final biomarkers by drawing a characteristic area under the cumulative curve of the random forest model. As shown in Figure 3C, the AUC value reached one after adding the second biomarker and stopped increasing when other new substances were added. Therefore, we screened the top two metabolites as biomarkers, including Neg_00510, which is SM 12:1;2O/30:0, and Pos_00557, which is TG 60:3|TG 18:0_24:1_18.

After obtaining the biomarkers by two-step screening, we validated and evaluated them using a logistic regression model. Owing to the small sample size, we used a grid search to determine the optimal model parameters for the logistic regression. We found that the biomarkers distinguished the two sample types sufficiently well and that the model parameters did not have a significant effect. Moreover, using

https://doi.org/10.1021/acs.jproteome.3c00527
J. Proteome Res. XXXX, XXX, XXX−XXX

the optimal parameters, we used the leave-one-out method to cross-validate and obtain the prediction results of the model. Figure 4C,D shows the confusion matrix of the model prediction results, and all of the test samples using the leave-one-out cross validation were predicted correctly. We get the final scores of the model as follows: accuracy: 1.0, precision: 1.0, recall: 1.0, F1 score: 1.0. A final score for each model was also observed. The values of these metrics showed excellent model performance for the evaluated metrics, indicating its high prediction accuracy.

The model parameters obtained from training were extracted according to the receiver operating characteristic plot of this model (Figure 4E), as shown in Figure 4F. The final logistic regression model obtained was as follows:

$$F = \text{sigmoid}(4.90475114e-16 + (-1.01511110e-07) * \text{Neg\_00510} + 5.24744164e-07 * \text{Pos\_00557})$$

The sigmoid function was $f(x) = \frac{1}{1+e^{-x}}$, and an image of the sigmoid function could be observed to determine the implementation of the classification model. The classification cutoff was 0.5 by default, and the samples with *F*-values greater than 0.5, calculated according to the model formula above, were classified into the EC group. Samples with *F*-values less than 0.5 were classified into the NTEC group. The tumor regression grades of our selected neoadjuvant therapy groups were all <4; therefore, neoadjuvant chemotherapy combined with immunotherapy was effective for all NTEC groups, and the model can effectively distinguish between the NTEC and EC groups. Therefore, we determined whether neoadjuvant chemotherapy combined with immunotherapy is effective.

DISCUSSION

In this study, we compared the lipid compositions of patients in the neoadjuvant and surgery-only groups using UPLC-MS/MS-based untargeted metabolomics analysis and identified differential lipids. We then applied KEGG enrichment analysis to identify the differentially involved metabolic pathways. We developed predictive models to predict the efficacy of neoadjuvant combination therapy for ESCC from a new perspective. Based on these results, we inferred that patients in the neoadjuvant therapy group experienced significant changes in glycerophospholipid metabolism, sphingolipid signaling pathways, choline metabolism in cancer, cellular autophagy, and GPI-anchored biosynthesis.

GPI-APs are modified proteins attached to the cell membrane by GPI-anchored proteins that bind to the plasma membrane in a noncovalent manner through the anchored lipid fraction. They are essential for cell adhesion, metabolism, proliferation, and immune regulation.[20] Some GPI-APs are involved in tumor development. cea, psa, CD59, and other GPI-APs directly promote cell proliferation, metastasis, and immune escape.[21] The enzyme involved in GPI anchoring is called GPI-transferase or GPI-T and is an essential factor affecting GPI anchoring. The mRNA level of GPAA1, a subunit of GPI-T, is elevated by 69% in head and neck squamous carcinomas and promotes gastric cancer.[22] GPI lipid remodeling plays an essential role in connecting GPI to cell membranes during the biosynthesis of GPI-anchored proteins.[23] Combined with our findings, the neoadjuvant therapy group may have affected lipids through neoadjuvant treatment, altering the binding of the GPI-APs lipid fraction to the plasma membrane, thus limiting tumor cell metabolism, proliferation, and immune escape.

Aphingolipid and choline metabolisms were altered in cancer tissues from the neoadjuvant therapy group. Choline is an anabolic substrate necessary for phospholipid synthesis. Choline kinase converts choline to phosphorylcholine, a precursor for the production of phosphatidylcholine, the major phospholipid component of membranes and a substrate for synthesizing lipid signaling molecules.[24,25] Cancer cells have high phosphorylcholine levels; choline kinase promotes phosphatidylcholine biosynthesis, and tumor cells have a high demand for this membrane phospholipid to promote cancer cell proliferation.[26] Sphingomyelin is a critical membrane component and a biologically active lipid mediator that regulates various biological functions.[27] Sphingomyelin is produced by converting phosphorylcholine to ceramide via sphingomyelin synthase (SMS). In membranes, SM is present in a restricted region known as the "SM-rich microdomain", which provides a special environment to regulate the binding of ligands to their receptors for the expression of cellular functions, such as proliferation, migration, and inflammation.[28] The SM cycle, in which ceramide and SM play opposing roles in cell death, survival, and proliferation, was proposed by Taniguchi et al. In cancer cells, ceramide is consistently expressed at low levels, and cancer cells inhibit the transfer of ceramide to SM or glucocerebrosides (GlcCer) via SMS and GlcCer synthase (GCS), thereby reducing the level of ceramide that induces cell death. The SM cycle is involved in programmed cell death (e.g., apoptosis, necrosis, and iron cell apoptosis) and the autophagy-dependent death of cancer cells. Therefore, regulating the ceramide/SM balance by increasing ceramide and decreasing SM can effectively inhibit tumor growth and proliferation.[29] We speculate that neoadjuvant therapy may function as a ceramide inducer of cell death by altering the choline metabolic pathway, reducing the total amount of phosphorylcholine, and decreasing the choline level in cancer cells, resulting in the downregulation of SM synthesis and upregulation of ceramide expression. Moreover, the synthesis of phosphatidylcholine and SM is reduced, and the raw materials for membrane synthesis required for cancer cell proliferation are insufficient, which, to some extent, also inhibits tumor cell proliferation and growth.

The model built by this analysis has some limitations owing to the small number of samples and the ability of some metabolites to better classify the two types of samples. However, the final two selected biomarkers were very good at classifying both types of samples, and the metrics were outstanding. The biomarkers selected by the integrated learning random forest model can guarantee a certain degree of stability, which is more stable than some individual classification models and is suitable for selecting biomarkers with a small sample size of histological data.

CONCLUSIONS

In this study, based on UPLC-MS/MS untargeted lipidomic analysis, we found that there were differences in lipids between the neoadjuvant therapy group and the surgery-only group, and after analyzing these lipids, we deduced that neoadjuvant therapy might achieve the effect of suppressing tumor proliferation and growth and then shrinking tumor foci by inhibiting the anchoring of GPI-APs, inhibiting the synthesis of choline and SM, and increasing programmed cell death of tumor cells, increasing the expression of ceramides through SM

https://doi.org/10.1021/acs.jproteome.3c00527
J. Proteome Res. XXXX, XXX, XXX−XXX

cyclic death and autophagy-dependent cell death, and decreasing the energy metabolism of tumor cells. Ceramide expression alters the energy metabolism of tumor cells, reduces the membrane raw materials required for proliferation to achieve the effect of inhibiting tumor proliferation and growth, and thus shrinks the tumor foci. We also developed a predictive model that offers a new possibility to predict the efficacy of neoadjuvant therapies by detecting two lipids (SM 12:1, 2O/30:0 and TG 60:3|TG 18:0_24:1_18).

AUTHOR INFORMATION

Corresponding Authors

Zhiyao Chen − *Department of Gastrointestinal and Esophageal Surgery, The Second Affiliated Hospital of Fujian Medical University, Quanzhou 362000, China*; Email: chenzyaoo@sina.com

Zhijun Huang − *Department of Gastrointestinal and Esophageal Surgery, The Second Affiliated Hospital of Fujian Medical University, Quanzhou 362000, China*; orcid.org/0000-0002-6666-6986; Email: huangzj@fjmu.edu.cn

Authors

Weijie Lin − *Department of Gastrointestinal and Esophageal Surgery, The Second Affiliated Hospital of Fujian Medical University, Quanzhou 362000, China*

Xianzhe Si − *Department of Gastrointestinal and Esophageal Surgery, The Second Affiliated Hospital of Fujian Medical University, Quanzhou 362000, China*

Zhihuang Zhao − *Department of Gastrointestinal and Esophageal Surgery, The Second Affiliated Hospital of Fujian Medical University, Quanzhou 362000, China*

Feng Chen − *Department of Gastrointestinal and Esophageal Surgery, The Second Affiliated Hospital of Fujian Medical University, Quanzhou 362000, China*

Jie Xu − *Department of Gastrointestinal and Esophageal Surgery, The Second Affiliated Hospital of Fujian Medical University, Quanzhou 362000, China*

Wenbo Huang − *Department of Gastrointestinal and Esophageal Surgery, The Second Affiliated Hospital of Fujian Medical University, Quanzhou 362000, China*

Jianqing Lin − *Department of Oncology, The Second Affiliated Hospital of Fujian Medical University, Quanzhou 362000, China*

Complete contact information is available at: https://pubs.acs.org/10.1021/acs.jproteome.3c00527

Author Contributions

[§]W.L. and X.S. contributed equally to this work.

Notes

The authors declare no competing financial interest.

We have uploaded the associated mass spectrometry data for the lipids via MetaboLights with the unique identifier MTBLS8815. The URL is www.ebi.ac.uk/metabolights/MTBLS8815.

ACKNOWLEDGMENTS

This study was supported by the Natural Science Foundation of Fujian Province (2021J01273), the Quanzhou High-level Talent Plan (2022C028R), and the Joint Funds for the innovation of science and Technology, Fujian province (2023Y9701). The authors would like to thank Editage (www.editage.cn) for English language editing. They would like to thank the Figdraw platform for giving us the material to draw the TOC.

REFERENCES

(1) Sung, H.; Ferlay, J.; Siegel, R. L.; et al. Global Cancer Statistics 2020: GLOBOCAN Estimates of Incidence and Mortality Worldwide for 36 Cancers in 185 Countries. *Ca-Cancer J. Clin.* **2021**, *71*, 209−249.

(2) Smyth, E. C.; Lagergren, J.; Fitzgerald, R. C.; et al. Oesophageal Cancer. *Nat. Rev. Dis. Primers* **2017**, *3*, 17048.

(3) Waters, J. K.; Reznik, S. I. Update on Management of Squamous Cell Esophageal Cancer. *Curr. Oncol. Rep.* **2022**, *24*, 375−385.

(4) Watanabe, M.; Otake, R.; Kozuki, R.; et al. Recent Progress in Multidisciplinary Treatment for Patients with Esophageal Cancer. *Surg. Today* **2020**, *50*, 12−20.

(5) Wu, Z.; Zheng, Q.; Chen, H.; et al. Efficacy and Safety of Neoadjuvant Chemotherapy and Immunotherapy in Locally Resectable Advanced Esophageal Squamous Cell Carcinoma. *J. Thorac. Dis.* **2021**, *13*, 3518−3528.

(6) Baba, Y.; Nomoto, D.; Okadome, K.; et al. Tumor Immune Microenvironment and Immune Checkpoint Inhibitors in Esophageal Squamous Cell Carcinoma. *Cancer Sci.* **2020**, *111*, 3132−3141.

(7) Yan, X.; Duan, H.; Ni, Y.; et al. Tislelizumab Combined with Chemotherapy as Neoadjuvant Therapy for Surgically Resectable Esophageal Cancer: A Prospective, Single-Arm, Phase II Study (TD-NICE). *Int. J. Surg.* **2022**, *103*, No. 106680.

(8) Kojima, T.; Shah, M. A.; Muro, K.; et al. Randomized Phase III KEYNOTE-181 Study of Pembrolizumab Versus Chemotherapy in Advanced Esophageal Cancer. *J. Clin. Oncol.* **2020**, *38*, 4138−4148.

(9) Sun, J. M.; Shen, L.; Shah, M. A.; et al. Pembrolizumab plus Chemotherapy Versus Chemotherapy Alone for First-Line Treatment of Advanced Oesophageal Cancer (KEYNOTE-590): a Randomised, Placebo-Controlled, Phase 3 Study. *Lancet* **2021**, *398*, 759−771.

(10) Bian, X.; Liu, R.; Meng, Y.; et al. Lipid Metabolism and Cancer. *J. Exp. Med.* **2021**, *218*, No. e20201606, DOI: 10.1084/jem.20201606.

(11) Dunn, G. P.; Bruce, A. T.; Ikeda, H.; Old, L. J.; Schreiber, R. D. Cancer Immunoediting: from Immunosurveillance to Tumor Escape. *Nat. Immunol.* **2002**, *3*, 991−998.

(12) Chen, Y.; Sui, M. Lipid Metabolism in Tumor-Associated Natural Killer Cells. *Adv. Exp. Med. Biol.* **2021**, *1316*, 71−85.

(13) Benny, S.; Mishra, R.; Manojkumar, M. K.; Aneesh, T. P. From Warburg Effect to Reverse Warburg Effect; the New Horizons of Anticancer Therapy. *Med. Hypotheses* **2020**, *144*, No. 110216.

(14) Luo, X.; Liu, J.; Wang, H.; Lu, H. Metabolomics Identified New Biomarkers for the Precise Diagnosis of Pancreatic Cancer and Associated Tissue Metastasis. *Pharmacol. Res.* **2020**, *156*, No. 104805.

(15) Ecker, J.; Benedetti, E.; Kindt, A. S. D.; et al. The Colorectal Cancer Lipidome: Identification of a Robust Tumor-Specific Lipid Species Signature. *Gastroenterology* **2021**, *161*, 910−923.e19e919.

(16) Yang, T.; Hui, R.; Nouws, J.; et al. Untargeted Metabolomics Analysis of Esophageal Squamous Cell Cancer Progression. *J. Transl. Med.* **2022**, *20*, 127.

(17) Lin, L.; Huang, Z.; Gao, Y.; et al. LC-MS Based Serum Metabonomic Analysis for Renal Cell Carcinoma Diagnosis, Staging, and Biomarker Discovery. *J. Proteome Res.* **2011**, *10*, 1396−1405.

(18) Vorkas, P. A.; Isaac, G.; Anwar, M. A.; et al. Untargeted UPLC-MS Profiling Pipeline to Expand Tissue Metabolome Coverage: Application to Cardiovascular Disease. *Anal. Chem.* **2015**, *87*, 4184−4193.

(19) Rice, T. W.; Ishwaran, H.; Ferguson, M. K.; Blackstone, E. H.; Goldstraw, P. Cancer of the Esophagus and Esophagogastric Junction: an Eighth ed. Staging Primer. *J. Thorac. Oncol.* **2017**, *12*, 36−42, DOI: 10.1016/j.jtho.2016.10.016.

(20) Lebreton, S.; Zurzolo, C.; Paladino, S. Organization of GPI-Anchored Proteins at the Cell Surface and Its Physiopathological Relevance. *Crit. Rev. Biochem. Mol. Biol.* **2018**, *53*, 403−419.

https://doi.org/10.1021/acs.jproteome.3c00527
J. Proteome Res. XXXX, XXX, XXX−XXX

(21) Gamage, D. G.; Hendrickson, T. L. GPI Transamidase and GPI Anchored Proteins: Oncogenes and Biomarkers for Cancer. *Crit. Rev. Biochem. Mol. Biol.* **2013**, *48*, 446−464.
(22) Zhang, X. X.; Ni, B.; Li, Q.; et al. GPAA1 Promotes Gastric Cancer Progression via Upregulation of GPI-Anchored Protein and Enhancement of ERBB Signalling Pathway. *J. Exp. Clin. Cancer Res.* **2019**, *38*, 214.
(23) Kinoshita, T.; Fujita, M. Biosynthesis of GPI-Anchored Proteins: Special Emphasis on GPI Lipid Remodeling. *J. Lipid Res.* **2016**, *57*, 6−24.
(24) Ridgway, N. D. The Role of Phosphatidylcholine and Choline Metabolites to Cell Proliferation and Survival. *Crit. Rev. Biochem. Mol. Biol.* **2013**, *48*, 20−38.
(25) Sonkar, K.; Ayyappan, V.; Tressler, C. M.; et al. Focus on the Glycerophosphocholine Pathway in Choline Phospholipid Metabolism of Cancer. *NMR Biomed.* **2019**, *32*, No. e4112.
(26) Glunde, K.; Penet, M. F.; Jiang, L.; Jacobs, M. A.; Bhujwalla, Z. M. Choline Metabolism-Based Molecular Diagnosis of Cancer: an Update. *Expert Rev. Mol. Diagn.* **2015**, *15*, 735−747.
(27) Hannun, Y. A.; Obeid, L. M. Sphingolipids and Their Metabolism in Physiology and Disease. *Nat. Rev. Mol. Cell Biol.* **2018**, *19*, 175−191.
(28) D'Angelo, G.; Moorthi, S.; Luberto, C. Role and Function of Sphingomyelin Biosynthesis in the Development of Cancer. *Adv. Cancer Res.* **2018**, *140*, 61−96.
(29) Taniguchi, M.; Okazaki, T. Role of Ceramide/Sphingomyelin (SM) Balance Regulated Through "SM Cycle" in Cancer. *Cell. Signalling* **2021**, *87*, No. 110119.

https://doi.org/10.1021/acs.jproteome.3c00527
J. Proteome Res. XXXX, XXX, XXX−XXX